DELIVERABLE REPORT

Deliverable no. / title:	D3.3 Scaling strategies 1
Lead beneficiary:	CNRS - LRCS
Nature of deliverable:	
Dissemination level:	PU - public
Due date:	M21 / September 2021

Grant Agreement number:	875489
Project acronym:	SONAR
Project title:	Modelling for the search for new active materials for redox flow batteries
Funding scheme:	H2020-LC-BAT-2019
Coordinator:	Fraunhofer ICT Jens Noack **Tel:** 0049 721 4640 870 **E-mail:** jens.noack@ict.fraunhofer.de
Project website:	www.sonar-redox.eu

Disclaimer

This project has received funding from the European Union's Horizon 2020 research and innovation programme under Grant Agreement no. 875489. This report reflects only the authors' view. The funding agency is not responsible for any use made of the information it contains.

Table of contents

1 Introduction

In the workflow of the SONAR project, Work Package 3 (WP3 – CNRS) takes charge of developing the mesoscale kinetic Monte Carlo (kMC) model, which simulates the electrode process of the anode of methyl viologen (MV)/4-hydroxy-2,2,6,6-tetramethylpiperidin-1-oxyl (4-HO-TEMPO) redox flow battery (RFB) system. The kMC model developed by WP3 has applied a 3-dimensional grid configuration to illustrate each molecule's position. Each chemical or physical process in the system, such as molecule and ion displacement, electrochemical reaction, and adsorption/desorption, is identified as an event and assigned with an event rate. The event rate is calculated based on the event mechanism. The kMC algorithm selects executable events at each time step and evolves the system status according to the pre-set simulation conditions. Meanwhile, a double layer model is coupled with the kMC model to complete the simulation to take into consideration the electrostatic field distribution in the simulation box. For more detailed modelling methodology, please refer to Deliverable 3.1.

However, although the kMC model demonstrates substantial advantages in kinetic analysis, the simulation time range (nanoseconds) makes it challenging to be coupled with continuum and macroscale models. Furthermore, the mass transport driven by convection was not considered due to the modelling scale limitations, and the redundant displacement events are a significant waste of computational power. Therefore, the objective of Task 3.5 is to develop a series of up-scaling strategies to bridge the gap between microscale and macroscale models and simplify the mesoscale kMC model.

This document presents the first upscaling strategies in Task 3.5 regarding our mesoscale kMC model. In this first stage of upscaling strategy development, we intend to bridge the gap between the microscale model and macroscale model from two aspects, the Mean-Field approach (MF), to simplify the previous kinetic Monte Carlo model reported in Deliverable 3.1 and the Lattice Boltzmann Method (LBM) to account for the electrolyte fluid dynamics. For the Mean-Field approach side, the modelling objective is to reduce the computational cost, average the dynamic behavior and expand the simulation time range to macroscale levels. The present Lattice Boltzmann Method focuses on the fluid dynamic simulation, which can be further coupled with electrochemical reaction models to simulate the global behavior of the full-cell system.

2 Mean-Field approach

The Mean-Field theory is originated from physics and probability theories, which approximate a high-dimensional model to a lower-dimensional model by averaging over the dynamic values in the simulation [1].

In a high-dimensional model, the interactions between every component are considered, which makes it complicated to find the final solution. On the contrary, the Mean-Field approach averages the interactions to a single representable value and thus, simplify a multi-body problem into a single-body problem [2]. In this way, the Mean-Field approach is capable of simulating system behaviors with a relatively lower computational cost.

2.1 Methodology of Mean-Field approach

In our previous kinetic Monte Carlo model, the target system was the methyl viologen-based anolyte. The simulation grid is illustrated in 3D, allowing us to account for all the displacement of molecules and ions, representing the transport limitation near the electrode surface. However, the particle displacement is not our targeting event and is also highly expensive regarding the computational cost due to the significant number of particles in the model.

To simplify the kMC model, we built a 0D Mean-Field theory model by removing the simulation grid and considering no transport limitation during discharge. Furthermore, the electrical double layer model is also simplified since no more electrical field distribution can be obtained from the simulation grid. Only the compact layer model is kept, which considers the double layer region as a constant capacitor. Therefore, the current 0D Mean-Field approach only focuses on the variation of reaction kinetics during the discharge process.

The main reaction scheme is the oxidation of MV during the discharge process with the reaction rate $k_{MV_{ox}}$ as follow:

$$MV^{+} \xrightarrow{k_{MV_{ox}}} MV^{2+} + e^{-}. \tag{1}$$

The reaction rate $k_{MV_{ox}}$ is calculated through the Eyring equation, which takes the reorganization energy E_λ and the potential drop η through the compact layer as input. The formula is expressed as follows,

$$k_{MV_{ox}} = \kappa \frac{k_B T}{h} \exp\left(\frac{-E_\lambda + f(\sigma)}{RT}\right),$$
$$with\ f(\sigma) = F\eta. \tag{2}$$

In our kMC model, the reorganization energy is considered as the sum of the inner and outter reorganization energies. The value of inner reorganization energy is provided by WP2, and the outter reorganization energy is calculated based on the tunneling distance. However, long-

distance electron tunneling is no longer considered in the Mean-Field approach. Thus, only the inner reorganization energy is implemented in the model.

Regarding the surface charge density σ, we followed the same approach as in Deliverable 3.1, where

$$-\frac{\partial \sigma}{\partial t} = J_{inp} - J_{Far}, \tag{3}$$

and

$$J_{Far} = \frac{\sum \Delta Q}{A \sum \Delta t}. \tag{4}$$

For each iteration, the simulation clock is advanced by a time step $\Delta t = \frac{1}{k_{MV_{ox}}}$, and the charge transferred is ΔQ.

In the kMC model, The discharging process is also accompanied by the adsorption and the desorption process of methyl viologen molecules, which can be expressed as,

$$MV^{+}_{free} \overset{k_{adsp1}}{\Longleftrightarrow} MV^{+}_{adsorbed}, \tag{5}$$

$$MV^{2+}_{free} \overset{k_{adsp2}}{\Longleftrightarrow} MV^{2+}_{adsorbed}, \tag{6}$$

where the energy barrier does not differentiate the adsorption and desorption yet, which is in disagreement with experimental observations and will be improved in the future. Thus, the same reaction rate is taken both for forward and backward events in the kMC model. In the Mean-Field approach, this process is not included yet.

The initial condition of the simulation was set at 0 current density and 0 charge density on the electrode. The cut off condition is met when the faradaic current density J_{Far} equals to the input current density J_{inp}. Due to the discrete calculation at each iteration, the value of Faradaic current density J_{Far} is difficult to be exactly equal to the value of the input current density J_{inp}. Thus, the simulation system is considered to meet the steady-state when the Faradaic current J_{Far} falls in the range of input current density.

2.2 Results and discussions of Mean-Field approach model

We tested the Mean-Field model under galvanostatic conditions with different input current densities, which vary from 25 mA/cm^2 to 200 mA/cm^2. The results are presented in Figure 1.

Figure 1 a. represents the evolution of the Faradaic current density. Since the controlling factor for the Faradaic current density J_{Far} is the reaction rate it self, the evolution of J_{Far} follows the same trend for different input current densities. Higher J_{inp} meets faster the steady-state.

Figure 1 b. is the potential drop through compact layer η, which follows the same trend of the Faradaic current density J_{Far}.

Compared with results obtained from the previous kMC model, the simulation time range is primarily expanded, which could reach an even larger time scale in the future. On the contrary, the computational cost is vastly reduced. Each simulation takes only several minutes compared to a kMC simulation taking several days.

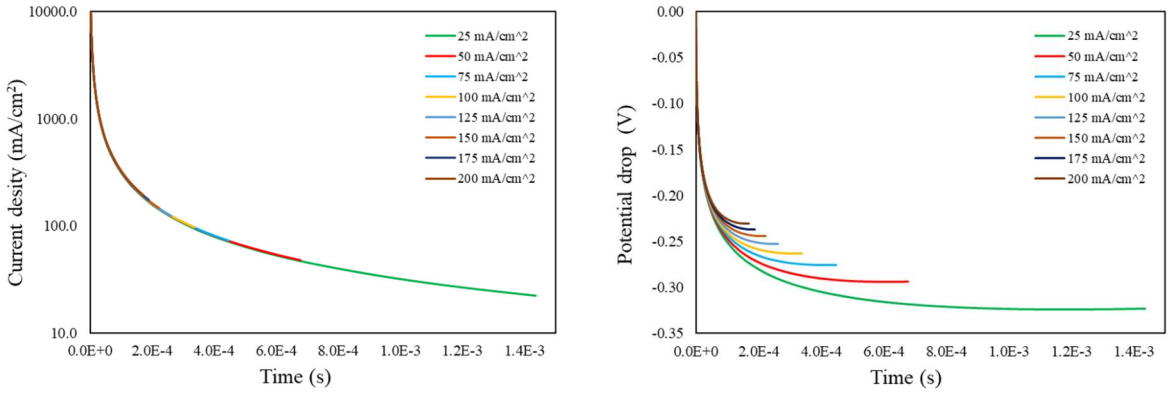

a. Faradaic current b. Potential drop

Figure 1. Mean-Field approach simulation results

This Mean-Field approach model is still under development. On the reaction side, only the electrochemical reaction is taken into consideration. The degradation event is not included yet. Furthermore, the present Mean-Field model does not include the impact of concentration yet, which is a critical parameter related to redox flow battery cells.

3 Lattice Boltzmann Method

Lattice Boltzmann Method (LBM) is an advanced mesoscale modeling approach well applied in computational fluid dynamics simulations. In classic continuum models, the primary independent variables are the pressure and the velocity of the fluid. However, LBM focuses on the particle velocity distribution functions (PDFs) [3]. As an efficient alternative to solve the Navier Stokes equation in complex geometries, LBM simulates the incompressible fluid flow by tracking the transport of these PDFs on a discrete Cartesian Lattice [4].

For the first stage of up-scaling strategies development, the LBM model is firstly adopted to investigate the physical properties of the carbon felt electrode and the electrolyte flow, such as the permeability of the felt electrode and the velocity of electrolyte under different inlet pressures.

Therefore, the present LBM model only simulates one fluid phase passing through the solid electrode structure. No chemical reaction is considered yet in this LBM model. However, in the future version of up-scaling strategies, we intend to implement a module simulating the reactions into the present LBM model.

3.1 Methodology of Lattice Boltzmann Method

In LBM, both fluid and electrode structures are mapped on a lattice. The fluid flow is demonstrated as the displacement of each particle, which is limited to specified directions [5]. A three-dimensional cubic lattice with 19 fixed velocity vectors (D3Q19) is applied to develop our LBM model.

According to the general idea of LBM, the displacement of each fluid particle can be described as follows,

$$f_i(x + e_i\delta t, t + \delta t) - f_i(x, t) = \Omega_i + F_b, \quad i = 0, 1, 2, \dots, 18 \tag{7}$$

where f_i is the particle distribution function, and e_i is the particle velocity at lattice location x at time t. The subscript i represents the velocity vector i around the grid unit, with 19 directions in our LBM approach. Ω_i is the collision operator at lattice node x at time t, which together with the particle distribution function f_i holds the system on Maxwellian equilibrium.

In the present work, a classic Bahtnagar-Gross-Krook (BGK) operator is chosen, which is expressed as:

$$\Omega_i^{BGK} = -\frac{1}{\tau}\left[f_i(x, t) - f_i^{eq}(x, t)\right], \tag{8}$$

where τ is the relaxation time related to the kinematic viscosity of the fluid V, which is calculated through $\mathrm{V} = c_s^2(\tau - \frac{1}{2})$ [4]. c_s is the lattice speed sound defined by $c_s = \frac{\frac{\delta t}{\delta x}}{\sqrt{3}}$, where δt and δx are the discrete-time step and length step, respectively, in the lattice standardized unit, *lu* [6].

The BGK operator is also called the single-relaxation-time (SRT) collision operator due to the dependence on only one parameter. The $f_i^{(eq)}$ is the particle distribution function at equilibrium state, which can be obtained through:

$$f_i^{(eq)}(x, t) = \omega_i \rho \left(1 + \frac{e_i \cdot v}{c_s^2} + \frac{(e_i \cdot v)^2}{2c_s^4} - \frac{v^2}{2c_s^2}\right), \tag{9}$$

where ω_i is the weighting factor for velocity vector i, where $w_i = 1/3$ for $i = 0$, $w_i = 1/18$ for $i = 1, \dots, 6$ and $w_i = 1/36$ for $i = 7, \dots, 18$. ρ is the density of the fluid. v is the dynamic fluid velocity. e_i is the discrete velocities defined as,

$$[\boldsymbol{e_0}, \boldsymbol{e_1}, \boldsymbol{e_2}, \boldsymbol{e_3}, \boldsymbol{e_4}, \boldsymbol{e_5}, \boldsymbol{e_6}, \boldsymbol{e_7}, \boldsymbol{e_8}, \boldsymbol{e_9}, \boldsymbol{e_{10}}, \boldsymbol{e_{11}}, \boldsymbol{e_{12}}, \boldsymbol{e_{13}}, \boldsymbol{e_{14}}, \boldsymbol{e_{15}}, \boldsymbol{e_{16}}, \boldsymbol{e_{17}}, \boldsymbol{e_{18}}]$$

=c

$$\begin{bmatrix} 0 & 1 & -1 & 0 & 0 & 0 & 0 & 1 & -1 & -1 & 1 & -1 & 1 & 1 & -1 & 0 & 0 & 0 & 0 \\ 0 & 0 & 0 & 1 & -1 & 0 & 0 & -1 & 1 & -1 & 1 & 0 & 0 & 0 & 0 & 1 & -1 & 1 & -1 \\ 0 & 0 & 0 & 0 & 0 & 1 & -1 & 0 & 0 & 0 & 0 & 1 & 1 & -1 & -1 & -1 & 1 & 1 & -1 \end{bmatrix}. \quad (10)$$

The representation of the discrete velocity is given in Figure 2.

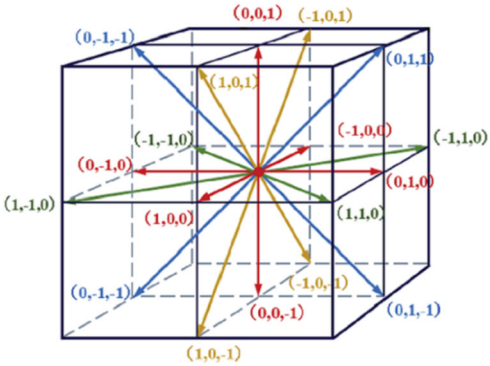

Figure 2. Illustration of D3Q19 LBM velocity vectors' direction [6].

The density and the velocity of the fluid are obtained from the moments of discrete distribution functions as:

$$\rho(x,t) = \sum_{i=0}^{n} f_i(x,t)\,, \quad (11)$$

$$\rho(x,t)v(x,t) = \sum_{i=0}^{n} e_i f_i(x,t). \quad (12)$$

In our simulation model, the system is exposed to external force F_b, which is the inlet pressure whose impact is added to the velocity of the fluid as

$$v^{eq}(x,t) = v(x,t) + \frac{\tau F_b}{\rho}. \quad (13)$$

Initially, we assumed the carbon felt electrode was filled with electrolyte with 0 velocity. Then, under the constant inlet pressure along the x-axis direction, the electrolyte flow reached a steady state where the velocity of the electrolyte flow remained constant.

The Lattice Boltzmann model is coded in C++ based on the Palabos package [7] and the previous work of Santos *et al* [8]. The post-processing of the result data was carried out on Paraview [9] and Python3.7 [10].

3.2 Workflow

In the first stage of developing the Lattice Boltzmann model, the simulation was carried out to investigate the physical properties of carbon felt electrodes. To start with, we generated different stochastic 3D electrode structures (*.raw file) through the Geodict FiberGeo module [11]. The porosity of the felt electrode took the previous work published by Gonzalez-Garcia *et al.* as reference [12]. They measured the porosity of carbon felt through the density method and the modeling of the resident time distribution method. The latter offered a more accurate porosity, which is around 0.98. Considering the variety of carbon felt products in the industry nowadays, we chose a series of porosity from 0.85 to 0.99, taking 0.02 as the interval (8 electrode structures in total).

The fiber diameter was extracted from the product datasheet of ZOLTEK OX felts [13]. Regarding the fiber shape, curved and straight circular fiber structures were mixed together with a ratio of 1:1. The partition of each type of fiber is presented in Table 1. The size of the felt structure is $500 \times 200 \times 200$ voxels with 1 µm as the unit length of the voxel. The electrode structure is then converted in *.dat format as the input for the LBM algorithm. Figure 3 is an example of generated electrode structure with a porosity of 0.95.

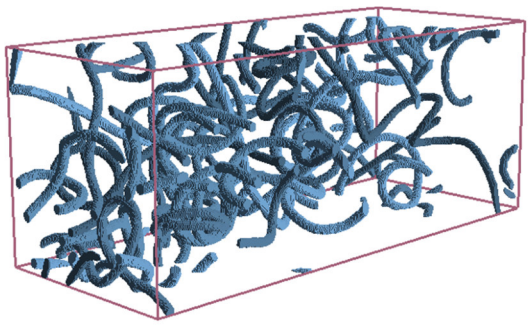

Figure 3. Geodict generated stochastic carbon felt electrode structure. Porosity $\varepsilon = 0.95$

Fiber diameter (µm)	Fiber shape	Partition (%)
7.5	Curve	25
7.5	Straight	25
8.5	Curve	25
8.5	straight	25

Table 1. Composition of the fiber electrode structure

3.3 Results and discussions of Lattice Boltzmann Method

The electrode performances of carbon felt are highly influenced by the structural and physical properties, such as fiber size, porosity, specific surface area, permeability, and electrical resistivity, determined by the fiber's geometry structure.

Through the modeling approach of LBM, we can investigate the fluid velocity and permeability of different electrode structures. The permeability k can be calculated in steady-state through

$$K = v \cdot \frac{\mu \delta x}{\Delta P}, \tag{14}$$

where μ is the dynamic viscosity of the electrolyte and ΔP is the pressure drop along the flow direction.

First, we tested the electrolyte flow passing through the electrode structure of $\varepsilon = 0.95$ (Figure 3) under different inlet pressures to validate the LBM model. The fluid flow direction is along the x-axis, and the periodic boundary conditions are applied on the side borders of the y-axis and z-axis. The velocity field obtained under the pressure of 0.005 *lu.* is shown in Figure 4 as an example. In the void region, the fluid velocity is higher compared with the velocity in dense fiber regions.

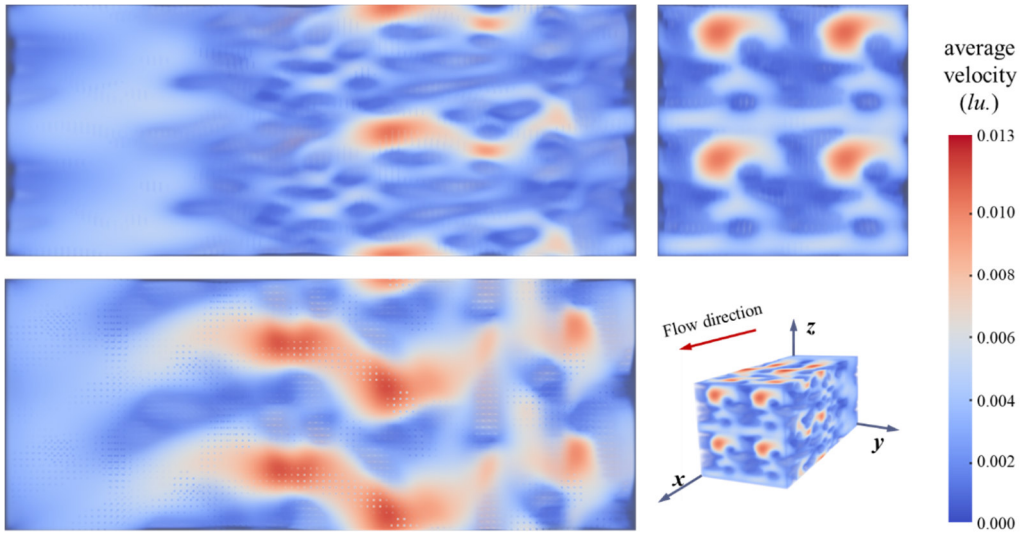

Figure 4. Velocity field illustration. $\varepsilon = 0.95$ and the inlet pressure equals 0.005 *lu.*

Figure 5 presents the relation between permeability, fluid velocity, and inlet pressures for the same electrode structure. As can be observed from the plot, permeability does not vary along with the increasing inlet pressure, which is in agreement with practical knowledge. Furthermore, as

permeability is one of the physical properties only related to the fibrous structure, changing operational conditions do not impact the permeability calculations. On the other hand, the fluid velocity is proportional to the inlet pressure, demonstrated as a linear relation in Figure 5, which is also in agreement with common knowledge.

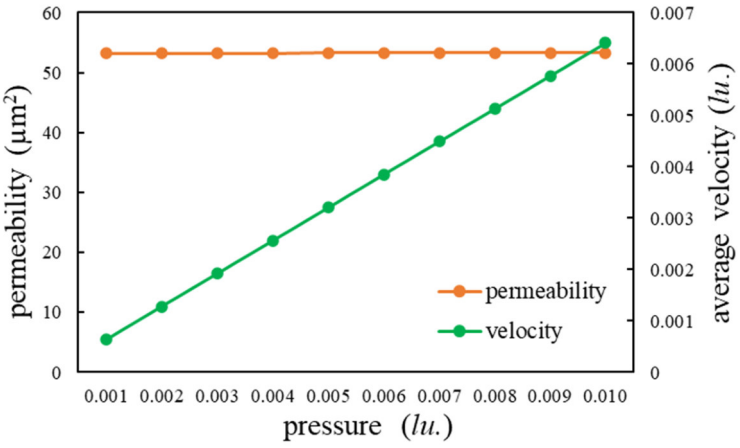

Figure 5. permeability and velocity evolution based on inlet pressure

Secondly, we investigated the relationship between electrode porosity, fluid velocity, and permeability. The performances of felt electrode structures with different porosities were tested under the same simulation conditions, where the inlet pressure was set at 0.005 *lu.*

Figure 6 presents the simulation results, where Figure 6 a. presents the permeability of different electrode structures under the same inlet pressure, and Figure 6 b. presents the average velocity of the electrolyte flow in different fibrous structures. The average velocity is obtained from Eq.13 and the permeability is calculated through Eq.14, which follows the trend of the average velocity curve.

Under the same inlet pressure, the electrode structure with higher porosity demonstrates a higher permeability in general (Figure 6 a.). However, exceptions exist at $\varepsilon = 0.89$ and $\varepsilon = 0.93$. The reason behind these exceptions is the heterogeneity of the stochastic generated electrode structure. The program Geodict verified the global porosity when processing. However, the local porosity in the final electrode structure could vary a lot, which causes the exception point at $\varepsilon = 0.89$ and $\varepsilon = 0.93$. Fortunately, increasing the sample numbers can reduce the problem of heterogeneity. Compared with the value measured by Gonzalez-Garcia *et al.* ($K = 293\ \mu m^2$ for an electrode with porosity $\varepsilon = 0.98$) [12], the permeability obtained from the LBM model falls in the same range ($K = 271\ \mu m^2$ at the point of porosity $\varepsilon = 0.99$).

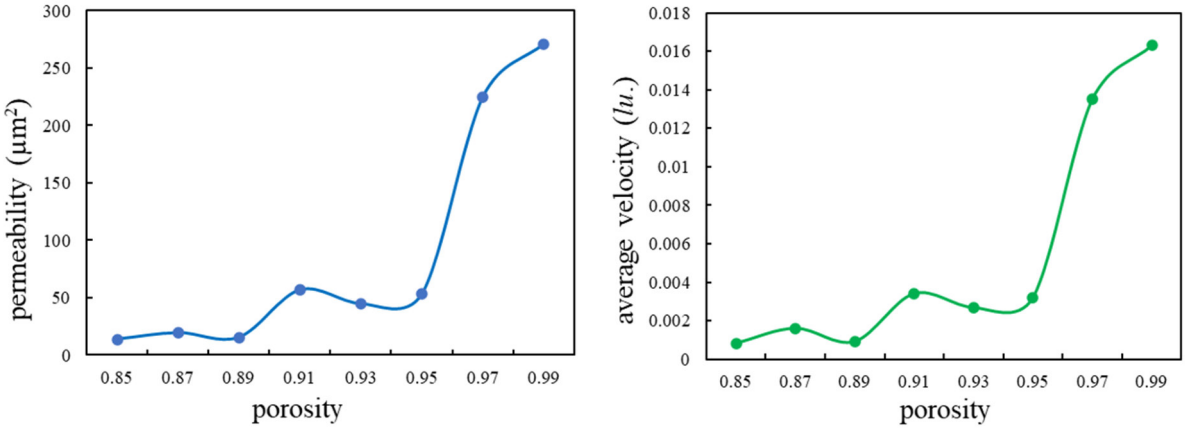

a. Relative permeability (μm²) b. Average velocity (*lu.*)

Figure 6. Permeability and average velocity obtained from LBM model based on different porosity of electrode structure.

Furthermore, we also investigated the impact of fiber shape on electrode permeability. Three different electrode structures were generated with the same porosity of $\varepsilon = 0.95$ and presented in Figure 7. These three different shaped fibrous structures were tested through the LBM model with the same inlet pressure. It is noticed from the simulation results that straight fiber offers the highest permeability and the mixed fiber demonstrated the lowest permeability. The reason could be the pore-size distribution and the tuotorsity factor in the electrode structure, which requires further investigations.

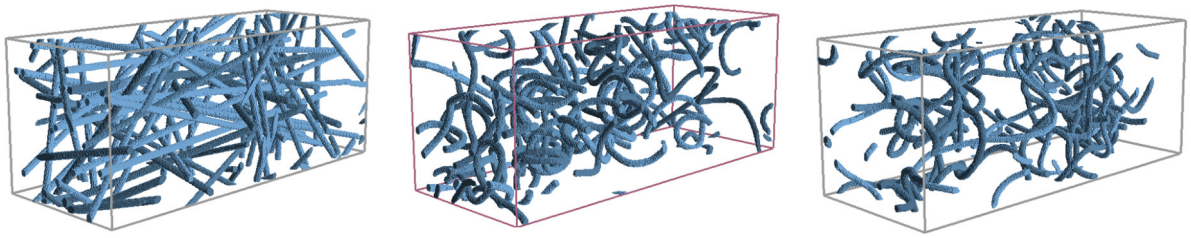

a. 100% straight fiber

$K = 655\ \mu m^2$

$v^{eq} = 0.0394\ lu.$

b. 50% straight fiber and 50% curved fiber

$K = 53.3\ \mu m^2$

$v^{eq} = 0.0032\ lu.$

c. 100% curved fiber

$K = 55\ \mu m^2$

$v^{eq} = 0.0194\ lu$

Figure 7. Illustration of different shaped felt structures and the simulated permeability.

4 Conclusions and perspectives

To conclude, this deliverable report presents two up-scaling strategies focusing on different aspects. First, the mean-field approach simulated the evolution of reaction kinetics while neglecting the molecule displacement. In this way, the MF approach simplified the kinetic Monte Carlo model, which offers a promising possibility of passing data to a higher modelling scale more efficiently. Second, the Lattice Boltzmann Method model simulates the steady-state when electrolyte flow passing through the carbon felt electrodes. The permeability of different felt structures is obtained and compared with previous literature and met in great agreement through the simulation.

Regarding the future development of up-scaling strategies, we intend to accomplish the calculation of the LBM model by including the electrochemistry reactions and mass transport process. Furthermore, the mean-field approach also needs to include more electrode processes, such as adsorption and desorption. To develop fully functional up-scaling strategies, more collaboration work with WP4 and WP5 will also be carried out in the future.

5 References

[1] A. Wipf, "Mean Field Approximation," in *Statistical Approach to Quantum Field Theory: An Introduction*, Berlin, Heidelberg: Springer Berlin Heidelberg, 2013, pp. 119–148.

[2] B. Andreaus and M. Eikerling, "Active site model for CO adlayer electrooxidation on nanoparticle catalysts," *J. Electroanal. Chem.*, vol. 607, no. 1–2, pp. 121–132, 2007, doi: 10.1016/j.jelechem.2007.02.020.

[3] A. Xu, W. Shyy, and T. Zhao, "Lattice Boltzmann modeling of transport phenomena in fuel cells and flow batteries," *Acta Mech. Sin. Xuebao*, vol. 33, no. 3, pp. 555–574, 2017, doi: 10.1007/s10409-017-0667-6.

[4] Y. H. Qian, D. D'Humières, and P. Lallemand, "Lattice bgk models for navier-stokes equation," *Epl*, vol. 17, no. 6, pp. 479–484, 1992, doi: 10.1209/0295-5075/17/6/001.

[5] P. K. Sinha, P. P. Mukherjee, and C. Y. Wang, "Impact of GDL structure and wettability on water management in polymer electrolyte fuel cells," *J. Mater. Chem.*, vol. 17, no. 30, pp. 3089–3103, 2007, doi: 10.1039/b703485g.

[6] A. Shodiev *et al.*, "Insight on electrolyte infiltration of lithium ion battery electrodes by means of a new three-dimensional-resolved lattice Boltzmann model," *Energy Storage Mater.*, vol. 38, no. February, pp. 80–92, 2021, doi: 10.1016/j.ensm.2021.02.029.

[7] J. Latt *et al.*, "Palabos: Parallel Lattice Boltzmann Solver," *Comput. Math. with Appl.*, vol.

81, pp. 334–350, 2021, doi: https://doi.org/10.1016/j.camwa.2020.03.022.

[8] J. E. Santos, M. Prodanović, C. J. Landry, and H. Jo, "Determining the Impact of Mineralogy Composition for Multiphase Flow through Hydraulically Induced Fractures," in *Unconventional Resources Technology Conference, Houston, Texas, 23-25 July 2018*, 2018, pp. 2542–2556.

[9] J. Ahrens, B. Geveci, and C. Law, "ParaView: An End-User Tool for Large-Data Visualization," 2005.

[10] G. van Rossum, "Python tutorial, May 1995," *CWI Rep. CS-R9526*, no. CS-R9526, pp. 1–65, 1995, [Online]. Available: http://oai.cwi.nl/oai/asset/5007/05007D.pdf.

[11] "FiberGeo handbook." GeoDict 2021 from Math2Market Gmbh, Germany, doi: https://doi.org/10.30423/userguide.geodict2021-FiberGeo2021.

[12] J. González-García, P. Bonete, E. Expósito, V. Montiel, A. Aldaz, and R. Torregrosa-Maciá, “Characterization of a carbon felt electrode: Structural and physical properties,” *J. Mater. Chem.*, vol. 9, no. 2, pp. 419–426, 1999, doi: 10.1039/a805823g.

[13] Toray group, "Commercial Carbon Fiber," 2021. https://zoltek.com/products/px35/.